Stability of steel struts with externally anchored prestressed cables

M. Ahmer Wadee[a], Nicolas Hadjipantelis[a,*], J. Bruno Bazzano[b], Leroy Gardner[a], Jose A. Lozano-Galant[c]

[a]*Department of Civil and Environmental Engineering, Imperial College London, South Kensington Campus, London, SW7 2AZ, UK*
[b]*Instituto de Estructuras y Transporte, Facultad de Ingeniería, Universidad de la República, Julio Herrera y Reissig 565, 11300, Montevideo, Uruguay*
[c]*Department of Civil Engineering, University of Castilla-La Mancha, Av Camilo Jose Cela SN, 13071, Ciudad Real, Spain*

Abstract

Externally anchored prestressed cables can be employed to enhance the stability of steel truss compression elements significantly. To demonstrate this concept, a system comprising a tubular strut subjected to an external compressive load and a prestressed cable anchored independently of the strut is studied. Energy methods are utilized to define the elastic stability of the perfect and imperfect systems, after which the first yield and rigid–plastic responses are explored. The influence of the key controlling parameters, including the length of the strut, the axial stiffness of the cable and the initial prestressing force, on the elastic stability, the inelastic response and the ultimate strength of the system is demonstrated using analytical and finite element (FE) models. To illustrate the application of the studied structural concept, FE modelling is employed to simulate the structural response of a prestressed hangar roof truss. A nearly two-fold enhancement in the load-carrying capacity of the truss structure is shown to be achieved owing to the addition of the prestressed cable.

Keywords: analytical modelling, energy methods, finite element modelling, prestressing, stability, steel structures

1. Introduction

Long-span steel trusses offer highly-efficient solutions for the design of large column-free spaces, such as sports stadia, aircraft hangars and industrial warehouses. However, with increasing span length, the self-weight of the trusses becomes a considerable proportion of the overall design loading. Significant material savings, and therefore self-weight

*Corresponding author
Email addresses: a.wadee@imperial.ac.uk (M. Ahmer Wadee), n.hadjipantelis15@imperial.ac.uk (Nicolas Hadjipantelis), bbazzano@fing.edu.uy (J. Bruno Bazzano), leroy.gardner@imperial.ac.uk (Leroy Gardner), JoseAntonio.Lozano@uclm.es (Jose A. Lozano-Galant)

reductions, can be achieved by the addition of prestressed high-strength steel cables in conjunction with conventional tubular truss components. Practical applications of prestressed steel trusses include the Ilshin Textile Factory in Changshu, China and the reconfiguration of the Sydney Olympic Stadium, Australia, shown in Figs. 1(a) and (b) respectively [1]. In these cases, substantial self-weight and time savings, improved construction safety and



(a) Ilshin Textile Factory (80 m clear span) in Changshu, China (b) Sydney Olympic Stadium (114 m clear span) in Australia

Figure 1: Structural applications of prestressed steel trusses [1].

increased structural performance have been reported.

In such trusses, the prestressed cables induce internal forces within the truss structure that counteract the subsequently applied external loading. Meanwhile, the cables carry loads through catenary action and control self-weight deflections. However, when the direction of external loading is such that an already prestressed (pre-compressed) element is further compressed, a reduction in performance can result. Crucial to whether or not this will be the case is the way in which the prestressing cables are anchored – either against the structure itself (*i.e.* mutually equilibrating) or externally anchored. The former case was explored in [2], while the latter case is studied herein.

The concept of prestressing steel structures was first investigated by Magnel [3], who suggested that considerable material and therefore cost savings can be achieved from the utilization of prestressed high-strength steel cables in conjunction with structural mild steel members. Subsequent research has focused on prestressed hot-rolled [4, 5, 6, 7] and cold-formed [8, 9, 10] steel beams, stayed columns [11, 12, 13, 14, 15], trusses [16, 17, 18, 19] and stressed-arch frames [20, 21].

More recently, an extensive experimental programme on the performance of prestressed high strength steel arched trusses has been conducted by Afshan *et al.* [22], with the components of the trusses tested individually in tension and compression [23]. To investigate the mechanical behaviour of individual prestressed steel elements comprising tubular steel members with internal prestressing cables, analytical, numerical and experimental work has also been conducted by Gosaye *et al.* [24, 2]. When subjected to tension, the studied cable-in-tube systems have demonstrated increased member strength and stiffness [24]. However, the presence of prestress can become detrimental when the steel elements are subjected to external compressive forces [2].

In contrast with the aforementioned cable-in-tube systems, in which the prestressed cables were anchored at the two member ends, in the steel truss members studied herein

the cables are anchored externally. A practical example of the studied structural concept is shown in Fig. 2(a), where the prestressed cable is housed within the tubular top chord of the roof truss of an aircraft hangar and is attached to anchorage blocks at ground level. In

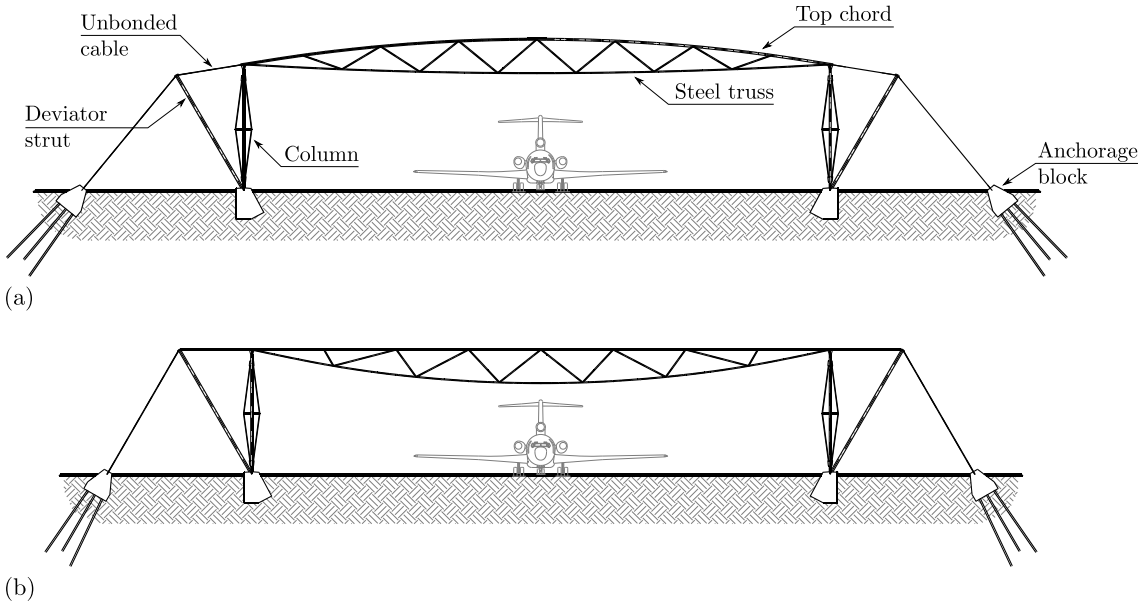


Figure 2: Roof truss in a hypothetical aircraft hangar with an externally anchored cable: (a) convex and (b) flat top chord profiles.

this case, the convex profile of the top chord results in a downwards force on the truss that is proportional to the prestressing force in the cable. This can be beneficial for trusses in geographical locations where design is governed by uplift wind loads. On the other hand, when gravity loads govern the design, a flat profile may be chosen for the top chord, as illustrated in Fig. 2(b); in this manner, no vertical forces are induced in the truss elements during prestressing.

A study investigating the inherent stabilizing action offered by the presence of externally anchored prestressed cables, which are encased within steel truss compression elements, is presented currently. It is demonstrated that the geometric stiffness of the cable can provide effective bracing for these members, thus enhancing their buckling resistance. Consequently, more slender elements can be employed in the design with the commensurate benefits of reducing structural self-weight and material consumption. The elastic stability of an idealized externally anchored strut is examined first using energy methods. This is performed for both the perfect and the imperfect systems. A numerical example demonstrating the elastic response of the system under different configurations and loading conditions is also presented. Subsequently, the first yield, rigid–plastic and ultimate behaviour of the members are examined. Finite element models are also developed to verify the behaviour of externally anchored truss elements and to simulate the response of a sample prestressed hangar roof truss.

2. Elastic stability of externally anchored cable-in-tube system

Following the description of the externally anchored, prestressed cable-in-tube, structural system, the elastic stability of both the perfect and the imperfect systems is studied presently. A numerical example is subsequently presented.

2.1. System characteristics

The elastic stability of the idealized structural system shown in Fig. 3 is studied herein. The system comprises a simply-supported tubular strut element that is subjected to an axial compressive force P. The strut houses a prestressed cable that is anchored externally, *i.e.* independently from the strut, such that no anchoring force is introduced into the strut due to the prestressing. Otherwise, if the cable were self-anchored, *i.e.* anchored directly to the strut, the prestressing would not contribute towards the stability of the strut; in such systems, the elastic critical buckling load is independent of the prestressing force [2, 23].

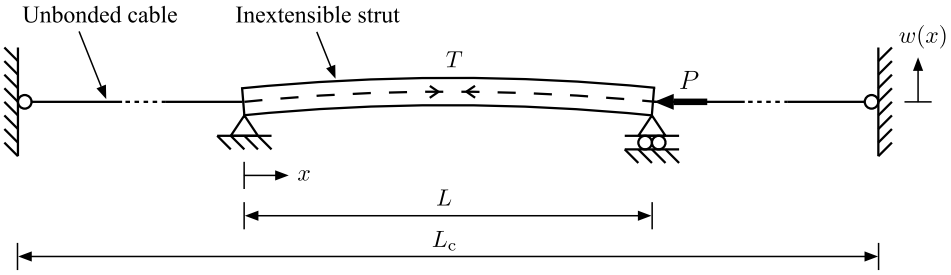


Figure 3: Initial geometry of the externally anchored, prestressed cable-in-tube, structural system.

The strut element is prismatic and of length L, constant cross-sectional area A and second moment of area I about its strong axis of bending. The strut material is assumed to be linearly elastic, homogeneous and isotropic with Young's modulus E. It should be noted presently that the strut is assumed to be inextensible; hence, only bending deformations are considered. Furthermore, an initial bowing imperfection affine to the critical buckling eigenmode is assumed to be present along the member. Thus, in the unstressed configuration, the centreline of the member has a half-sine wave profile of amplitude ϵL, where ϵ is a non-dimensional measure of the imperfection magnitude.

The cable is of initial length L_c, cross-sectional area A_c and carries a pre-tensioning force T. The cable material is also linearly elastic, homogeneous and isotropic with Young's modulus E_c. However, it is assumed that the cable has no bending stiffness; hence, it is able to carry only axial forces in tension. Note also that the cable is considered to be unbonded, *i.e.* free to elongate along the entire length of the member [8], while the contact between the strut and the cable is assumed to be frictionless. Moreover, the cable is constrained to be located at the centreline of the strut by means of closely-spaced collars [2, 23], such that throughout loading its shape coincides with the deflected shape of the strut.

2.2. Imperfect system

The configuration of the structural system is defined in terms of the lateral deflection $w(x)$, as shown in Fig. 3, where x is measured along the line between the supports of the strut, such that $x = [0, L]$. For the simply-supported strut, and considering the lowest buckling mode, $w(x)$ can be taken as a sinusoidal function, thus:

$$w(x) = QL \sin \frac{\pi x}{L}, \tag{1}$$

where Q is a generalized coordinate. In the same manner, the initial imperfection profile $w_\epsilon(x)$ of the system is defined using:

$$w_\epsilon(x) = \epsilon L \sin \frac{\pi x}{L}. \tag{2}$$

The elastic stability of the system is investigated using the principle of minimum total potential energy V [25], which comprises contributions from the bending strain energy stored in the strut U_b and the axial strain energy stored in the cable U_c, minus the work done by the axial compressive force P, which is the loading parameter, *i.e.*:

$$V = U_\mathrm{b} + U_\mathrm{c} - P\mathcal{E}, \tag{3}$$

where $\mathcal{E}$ is the longitudinal displacement of the sliding support.

2.2.1. Bending strain energy in strut

Assuming moderately large rotations, the bending strain energy stored in an inextensible imperfect elastic strut is [25]:

$$U_\mathrm{b} = \int_0^L \frac{1}{2} EI \left(w'' - w_\epsilon''\right)^2 \left[1 + \left(w' - w_\epsilon'\right)^2\right] \mathrm{d}x, \tag{4}$$

where primes denote differentiation with respect to x.

2.2.2. Axial strain energy in cable

The axial strain energy density in the cable is given by the expression:

$$\mathrm{d}U_\mathrm{c} = \frac{1}{2} E_\mathrm{c} \varepsilon_\mathrm{c}^2, \tag{5}$$

where ε_c is the total axial strain in the cable. This is equal to the initial strain introduced by the prestressing force T plus the strain due to the stretching of the cable during loading, which is induced owing to the lateral deflection of the strut. Given the inextensible nature of the strut, the strain due to the stretching of the cable is simply equal to the total longitudinal displacement of the sliding support $\mathcal{E}$ divided by the original length of the cable L_c. Hence, the total axial strain in the cable is given by:

$$\varepsilon_\mathrm{c} = \frac{T}{E_\mathrm{c} A_\mathrm{c}} + \frac{\mathcal{E}}{L_\mathrm{c}}, \tag{6}$$

where $\mathcal{E}$ can be determined using the expression for the inextensible strut end displacement for moderately large displacements [25], *i.e.*:

$$\mathcal{E} = \int_0^{\mathrm{L}} \left[\frac{1}{2} \left(w'^2 - w_\epsilon'^2 \right) + \frac{1}{8} \left(w'^4 - w_\epsilon'^4 \right) \right] \mathrm{d}x. \tag{7}$$

Combining Eqs. (5)–(7) and integrating through the cable volume, the total axial strain energy in the cable is obtained thus:

$$U_{\mathrm{c}} = \frac{k_{\mathrm{c}}}{2} \left\{ \int_0^{\mathrm{L}} \left[\frac{1}{2} \left(w'^2 - w_\epsilon'^2 \right) + \frac{1}{8} \left(w'^4 - w_\epsilon'^4 \right) \right] \mathrm{d}x + \frac{T}{k_{\mathrm{c}}} \right\}^2, \tag{8}$$

where k_{c} is the axial stiffness of the cable, *i.e.*:

$$k_{\mathrm{c}} = \frac{E_{\mathrm{c}} A_{\mathrm{c}}}{L_{\mathrm{c}}}. \tag{9}$$

2.2.3. Work done by external load

Utilizing Eq. (7), the work done by the external load P is simply given by:

$$P\mathcal{E} = P \int_0^{\mathrm{L}} \left[\frac{1}{2} \left(w'^2 - w_\epsilon'^2 \right) + \frac{1}{8} \left(w'^4 - w_\epsilon'^4 \right) \right] \mathrm{d}x. \tag{10}$$

2.2.4. Total potential energy and equilibrium path

Substituting Eqs. (4), (8) and (10) into Eq. (3), the total potential energy in the imperfect system is thus:

$$\begin{aligned} V = {} & \frac{k_{\mathrm{c}}}{2} \left\{ \int_0^{\mathrm{L}} \left[\frac{1}{2} \left(w'^2 - w_\epsilon'^2 \right) + \frac{1}{8} \left(w'^4 - w_\epsilon'^4 \right) \right] \mathrm{d}x + \frac{T}{k_{\mathrm{c}}} \right\}^2 \\ & + \frac{1}{2} \int_0^{\mathrm{L}} \left\{ EI \left(w'' - w_\epsilon'' \right)^2 \left[1 + \left(w' - w_\epsilon' \right)^2 \right] - P \left[\left(w'^2 - w_\epsilon'^2 \right) + \frac{1}{4} \left(w'^4 - w_\epsilon'^4 \right) \right] \right\} \mathrm{d}x. \end{aligned} \tag{11}$$

Substituting Eqs. (1) and (2) into Eq. (11), utilizing Rayleigh's method [25] and neglecting the constant energy terms (which vanish upon differentiation with respect to Q for equilibrium in any case), the following one-dimensional expression for V as a function of the generalized coordinate Q is obtained:

$$\begin{aligned} V = {} & \frac{\pi^4 EI}{4L} (Q - \epsilon)^2 \left[1 + \frac{\pi^2}{4} (Q - \epsilon)^2 \right] + \frac{\pi^2 L}{4} Q^2 \left[T + \left(\frac{3T}{2} + k_{\mathrm{c}} L \right) \frac{\pi^2}{8} Q^2 \right] \\ & - \frac{P \pi^2 L}{4} Q^2 \left[1 + \frac{3\pi^2}{16} Q^2 \right]. \end{aligned} \tag{12}$$

Hence, by determining the condition for stationary V with respect to Q, the following equilibrium path of the imperfect system is obtained:

$$P \left(1 + \frac{3\pi^2}{8} Q^2 \right) = P_{\mathrm{E}} \frac{(Q - \epsilon)}{Q} \left[1 + \frac{\pi^2}{2} (Q - \epsilon)^2 \right] + T + \pi^2 \left(\frac{3T}{8} + \frac{1}{4} k_{\mathrm{c}} L \right) Q^2. \tag{13}$$

2.3. Perfect system

2.3.1. Fundamental path and critical buckling load

To analyse the stability of the perfect system, whereby no initial imperfections are present, the normalized imperfection amplitude ϵ in Eq. (12) is zero; hence, V becomes:

$$V = \frac{\pi^4 EI}{4L} Q^2 \left[1 + \frac{\pi^2}{4} Q^2\right] + \frac{\pi^2 L}{4} Q^2 \left[T + \left(\frac{3T}{2} + k_\mathrm{c} L\right) \frac{\pi^2}{8} Q^2\right] - \frac{P\pi^2 L}{4} Q^2 \left[1 + \frac{3\pi^2}{16} Q^2\right]. \tag{14}$$

Regarding the equilibrium of the perfect system, the first derivative of V with respect to Q gives a trivial fundamental equilibrium path $Q = 0$. In addition, by invoking the condition that at the critical buckling load P^C the second derivative of V with respect to Q is zero:

$$P^\mathrm{C} = P_\mathrm{E} + T, \tag{15}$$

where P_E is the Euler buckling load of the strut, thus:

$$P_\mathrm{E} = \frac{\pi^2 EI}{L^2}. \tag{16}$$

It is worth noting that, while being a function of the prestressing force, the critical buckling load is in fact independent of the axial stiffness of the cable.

2.3.2. Post-buckling path

The post-buckling equilibrium path of the perfect system can be determined by setting the imperfection amplitude ϵ in Eq. (13) equal to zero, thus:

$$P\left(1 + \frac{3\pi^2}{8} Q^2\right) = P^\mathrm{C} + \frac{\pi^2}{4}\left(2P_\mathrm{E} + \frac{3T}{2} + k_\mathrm{c} L\right) Q^2. \tag{17}$$

The post-buckling path can also be approximated using the perturbation method, *i.e.* the so-called "General Theory" developed by Thompson and Hunt [25]. To leading order in terms of Q, the General Theory approximation is given by:

$$P = P^\mathrm{C} + \frac{1}{2} \left.\frac{\mathrm{d}^2 P}{\mathrm{d}Q^2}\right|^\mathrm{C} Q^2, \tag{18}$$

which, in the neighbourhood of P^C, would agree with the exact expression for the post-buckling path, as given in Eq. (17).

2.3.3. Stability of post-buckling path

In terms of the current system, expressing V relative to the critical load P^C and truncating the resulting equation consistently gives:

$$\begin{aligned} V &= U_\mathrm{b} + U_\mathrm{c} - P^\mathrm{C}\mathcal{E} - (P - P^\mathrm{C})\mathcal{E} \\ &= \frac{\pi^4 L}{64}\left(P_\mathrm{E} + 2k_\mathrm{c} L\right) Q^4 - (P - P^\mathrm{C})\frac{\pi^2 L}{4} Q^2. \end{aligned} \tag{19}$$

Meanwhile, in terms of the General Theory [25]:

$$V = \frac{1}{24} V_{1111}^{\mathrm{C}} Q^4 + (P - P^{\mathrm{C}}) \frac{1}{2} V_{11}^{\prime \mathrm{C}} Q^2, \tag{20}$$

where the subscripts "1" denote the order of the partial derivative with respect to Q and the superscript "C" indicates that the term is evaluated at the critical point (*i.e.* $P = P^{\mathrm{C}}$). Hence, the coefficients V_{1111}^{C} and $V_{11}^{\prime \mathrm{C}}$ represent, to leading order, the contributions from the strain energy and the work done by load when evaluated at the critical load $P = P^{\mathrm{C}}$, respectively.

Comparing coefficients with respect to Q between Eqs. (19) and (20) directly leads to the expressions:

$$V_{1111}^{\mathrm{C}} = \frac{3\pi^4 L}{8} \left(P_{\mathrm{E}} + 2k_{\mathrm{c}} L \right), \quad V_{11}^{\prime \mathrm{C}} = -\frac{\pi^2 L}{2}, \tag{21}$$

which, according to the General Theory, comprise the key terms required to evaluate the curvature of the post-buckling path, *i.e.*:

$$\left. \frac{\mathrm{d}^2 P}{\mathrm{d} Q^2} \right|^{\mathrm{C}} = -\left. \frac{V_{1111}}{3V_{11}'} \right|^{\mathrm{C}} = \frac{\pi^4}{4} k_{\mathrm{b}} L + \frac{\pi^2}{2} k_{\mathrm{c}} L = \frac{\pi^4 k_{\mathrm{b}} L}{4} \left(1 + \frac{2\kappa}{\pi^2} \right), \tag{22}$$

where k_{b} is the bending stiffness of the strut and κ is the ratio of the cable to the strut stiffnesses, thus:

$$k_{\mathrm{b}} = \frac{EI}{L^3}, \quad \kappa = \frac{k_{\mathrm{c}}}{k_{\mathrm{b}}}. \tag{23}$$

Note that Eq. (22) can be substituted into Eq. (18) to obtain the General Theory expression for the post-buckling path.

The fact that the expression for the curvature of the post-buckling path is positive implies that the post-buckling response of the perfect system is stable. Meanwhile, the curvature of the post-buckling path is independent of the prestressing force T. It is worth noting that increasing the length of the strut L in turn decreases the first term of the curvature expression, but increases the effect of the second term; the overall effect of the strut length is investigated numerically in the following sub-section. Finally, as shown in Eq. (22), the post-buckling stability can be enhanced by increasing the axial stiffness of the cable, which in turn increases the relative stiffness parameter κ.

2.4. Numerical example

To investigate the structural behaviour of the studied system, a numerical example is presented below. For this purpose, the response of a sample system under different configurations and loading conditions is determined by utilizing the equilibrium path expressions derived in Sections 2.3.1–2.3.2 for the perfect cases and Section 2.2.4 for the imperfect cases. The properties of the sample system are given in Table 1. An initial prestressing force $T_0 = 1400$ kN is assumed.

The response of the sample perfect system is illustrated in Fig. 4(a), where the cross ($\times$) and circle ($\circ$) symbols indicate the Euler load P_{E} of the bare steel strut (*i.e.* with

Table 1: Geometric and material properties of the sample system.

Tube:	
Young's modulus, E	205 kN/mm^2
Second moment of area, I	22.6×10^6 mm^4
Length, L_0	7.5 m
Cable:	
Young's modulus, E_c	160 kN/mm^2
Cross-sectional area, A_c	1650 mm^2
Length, L_c	105 m

no cable present) and the critical load P^C of the prestressed system respectively. The fundamental and post-buckling equilibrium paths of the prestressed system are also shown. The post-buckling paths were determined using the principle of stationary total potential energy directly, denoted as "Full expression", and the General Theory approach; this was achieved by plotting Eqs. (17) and (18) respectively. As shown in Fig. 4(a), the equilibrium path from General Theory is slightly stiffer for moderately large displacements, but in the neighbourhood of $P = P^C$, the paths are practically coincident.

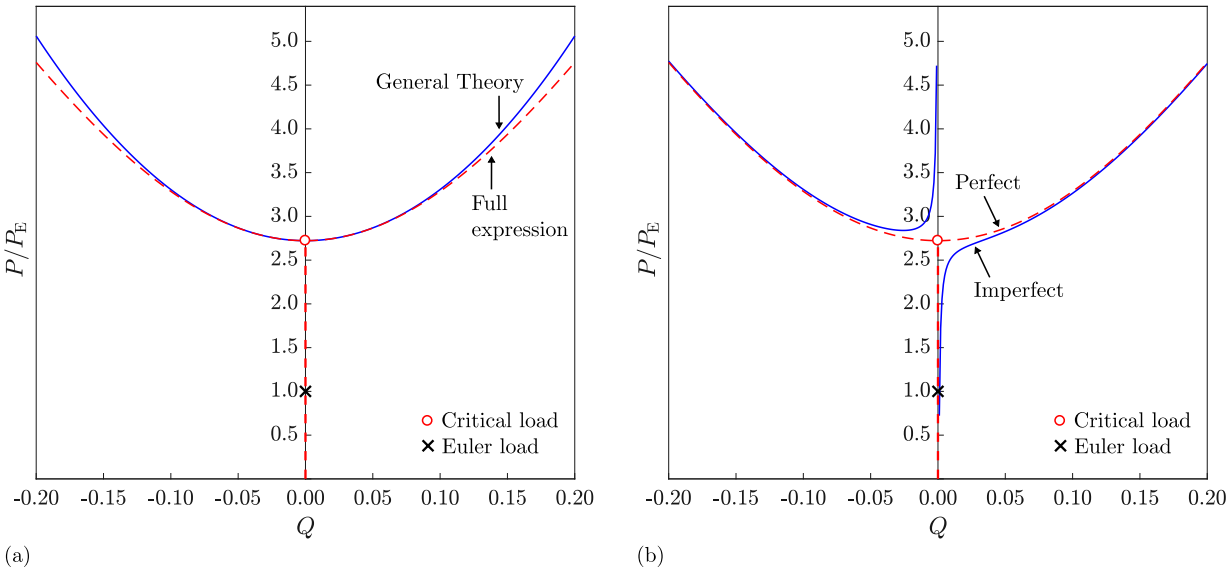


Figure 4: (a) Post-buckling equilibrium paths of the sample perfect system; (b) comparison between the equilibrium paths of the perfect and imperfect systems.

A comparison between the responses of the perfect and imperfect systems is shown in Fig. 4(b), where the asymptotic nature of the latter to the former is also demonstrated. The equilibrium path of the imperfect system was obtained using Eq. (13) with an initial normalized imperfection $\epsilon = 1/500$ being assumed.

The effect of increasing the initial prestressing force T while maintaining a fixed strut length $L = L_0$ is shown in Fig. 5(a). For this purpose, the sample perfect system was considered and the prestress level was varied from zero to $1.5T_0$ in steps of $0.5T_0$. As

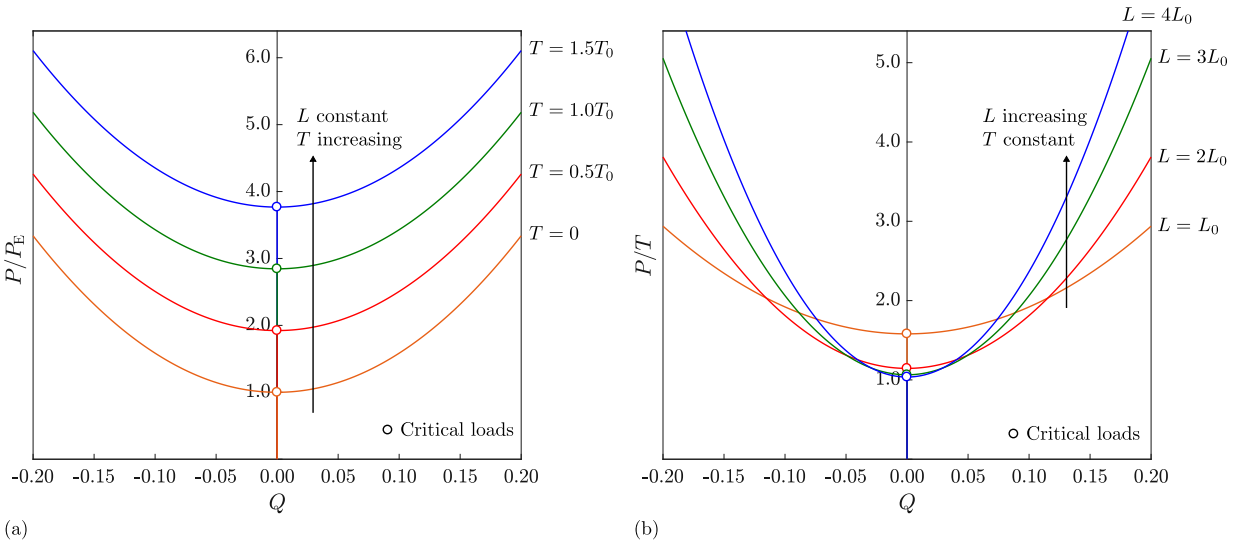


Figure 5: Effects of (a) increasing the prestressing force T while maintaining a fixed strut length $L = L_0$ and (b) increasing the strut length L while maintaining a fixed prestressing force $T = T_0$.

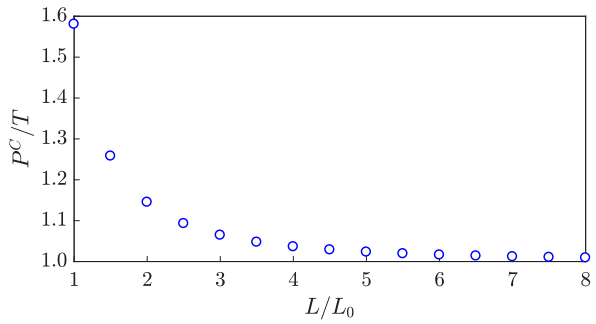


Figure 6: Variation of the normalized critical buckling load with respect to the length of the strut.

expected from Eq. (15), the higher the prestress level, the higher the critical buckling load of the system. Furthermore, it is observed that the post-buckling stability of the system is independent of the magnitude of the prestressing force.

In Fig. 5(b), the effect of varying the length of the strut L while keeping a constant initial prestressing force $T = T_0$ is shown. In this case, the strut length was increased from L_0 to $4L_0$ in steps of L_0. As expected, by increasing the length of the strut L, the critical buckling load of the system is reduced. Meanwhile, as discussed in Section 2.3.3, the post-buckling stability of the system is enhanced; this is indicated by the increased curvature of the post-buckling path. Of course, as demonstrated in Fig. 6 for various strut lengths, as the strut becomes longer, the critical load P^{C} converges to the initial prestress level T; this can be also be deduced by inspecting Eqs. (15) and (16).

3. Ultimate behaviour of externally anchored cable-in-tube system

In the present section, the first yield and rigid–plastic responses of the cable-in-tube system are studied. Initially, the occurrence of first yield at the most heavily stressed fibre of the strut is examined through extension of the well-known Perry–Robertson concept [26]. Subsequently, the formation and rotation of a plastic hinge at the midspan of the strut are studied by means of a rigid–plastic analysis.

Generally, the point of first yield is shown to be weakly dependent on the relative stiffness parameter κ, defined in Eq. (23). In contrast, it is demonstrated that κ can have a significant effect on the stability of the system after the point of first yield. Hence, a relationship is derived to estimate a limiting value of κ that determines whether the ultimate point is well predicted by the load corresponding to first yield or whether the response of the system remains stable as plasticity develops enabling higher loads to be sustained.

3.1. Occurrence of first yield

The derivation of the load at first yield considers the imperfect strut with the axial stiffness of the prestressed cable initially being included in the formulation. Subsequently, to offer a simpler and more direct expression for the determination of the first yield capacity, the axial stiffness of the cable is excluded from the formulation.

3.1.1. Including cable axial stiffness

To determine the first yield capacity of the cable-in-tube system, *i.e.* the applied axial load corresponding to the point of first yield P_1, the Perry–Robertson concept [26] is extended to include the effect of the addition of the prestressed cable. The formulation of the capacity is based on a first yield condition, which implies that the maximum stress level $\sigma_{\max}$ in the imperfect strut is equal to the yield stress f_{y}. The maximum stress $\sigma_{\max}$ evidently occurs at midspan $x = L/2$, where the strut is subjected to an axially compressive force P and a second-order bending moment M. Hence, based on Euler–Bernoulli beam theory:

$$\sigma_{\max} = \frac{P}{A} + \frac{Md}{I}, \tag{24}$$

where d is the distance from the centroid of the cross-section to the most heavily stressed fibre. Moreover, since:

$$M = -EI[w''(L/2) - w''_{\epsilon}(L/2)] \,, \tag{25}$$

by utilizing Eqs. (1), (2) and (16), this can be re-expressed, thus:

$$M = P_{\mathrm{E}} L(Q - \epsilon). \tag{26}$$

At this point, it is convenient to employ the non-dimensional parameters given in Table 2, where $r = \sqrt{I/A}$ is the radius of gyration of the cross-section of the strut. Based on

Table 2: Definitions of non-dimensional parameters.

Non-dimensional parameter:	Expression:
Normalized first yield capacity	$\chi = \dfrac{P_1}{Af_y}$
Strut slenderness	$\bar{\lambda} = \sqrt{\dfrac{Af_y}{P_E}}$
Normalized prestress level	$\tau = \dfrac{T}{Af_y}$
Normalized imperfection size	$\eta = \dfrac{\epsilon dL}{r^2}$
Normalized radius of gyration	$\rho = \dfrac{r}{d}\sqrt{\dfrac{f_y}{E}}$
Normalized midspan deflection	$q = \dfrac{Q}{\epsilon}$

these parameters alongside Eqs. (24) and (26), the buckling reduction factor χ can be obtained by invoking the first yield condition (*i.e.* $\sigma_{\max} = f_y$), thus:

$$\chi = 1 - \frac{\eta}{\lambda^2}(q-1). \tag{27}$$

To obtain the normalized midspan deflection q, the relationship between load P and lateral deflection Q of the imperfect system, as defined in Eq. (13), is employed. Hence, utilizing the normalized parameters given in Table 2 and truncating the ϵ^3 terms, Eq. (13) can be first re-expressed as a function of χ and then equated to Eq. (27) to obtain the following expression:

$$\begin{aligned}\left[1 - \frac{\eta}{\lambda^2}(q-1)\right]\left(\lambda^2 + \frac{3}{8}\eta^2\rho^2q^2\right) = \left(1 - \frac{1}{q}\right) + \left(\frac{\eta^2\rho^2}{2\lambda^2}\right)(q-1)(q-2) \\ + \tau\lambda^2 + \eta^2\rho^2\left(\frac{3\tau}{8} + \frac{\kappa}{4\pi^2\lambda^2}\right)q^2,\end{aligned} \tag{28}$$

which can be re-arranged in terms of q to give the following quartic equation:

$$\begin{aligned}\left(\frac{3\eta^3}{8}\right)q^4 + \left(\frac{3\eta^2}{8}\right)\left[\frac{4}{3} + \tau\lambda^2 + \frac{2\kappa}{3\pi^2} - \eta - \lambda^2\right]q^3 + \left(\frac{\eta\lambda^2}{\rho^2} - \frac{3\eta^2}{2}\right)q^2 \\ + \left(\frac{\lambda^2}{\rho^2}\right)\left[1 + \tau\lambda^2 - \lambda^2 - \eta + \frac{\eta^2\rho^2}{\lambda^2}\right]q - \frac{\lambda^2}{\rho^2} = 0.\end{aligned} \tag{29}$$

Equation (29) can be solved numerically to determine the value of the normalized lateral displacement q_1 at which first yield occurs. Finally, by substituting the value of q_1 into

Eq. (27), the buckling reduction factor of the system χ can be determined. The load corresponding to the point of first yield can then be calculated thus:

$$P_1 = \chi A f_y. \tag{30}$$

To investigate the effect of the strut slenderness, prestress level and cable stiffness on the capacity of the system, the aforementioned procedure is utilized to obtain the graphs presented in Fig. 7, where the dotted line represents the 'no cable' case (*i.e.* $\kappa = 0$ and $\tau = 0$). Note that in this example the normalized imperfection magnitude was defined using the Eurocode 3 designation [27], *i.e.* $\eta = \alpha(\bar{\lambda} - 0.2) \not< 0$, where $\alpha = 0.21$ for hot-rolled tubular members. The Young's modulus and yield stress of the steel strut were taken as $E = 210$ kN/mm^2 and $f_y = 275$ N/mm^2 respectively.

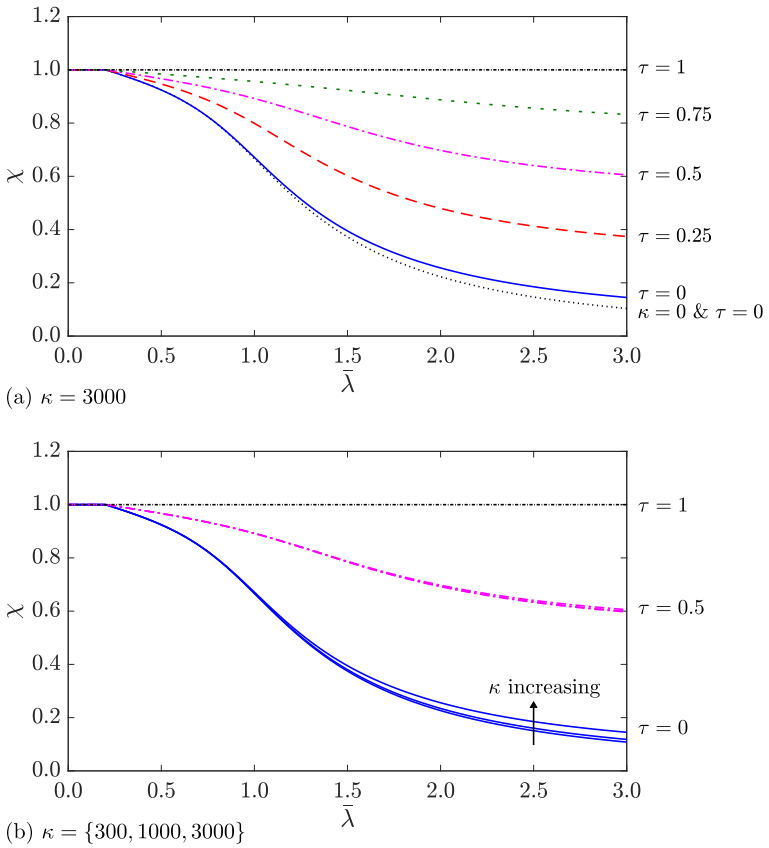


Figure 7: Variation of the buckling reduction factor χ, defined as the ratio of the first yield capacity to the squash load of the strut, with respect to the strut slenderness $\bar{\lambda}$ for different values of (a) normalized prestress levels τ and (b) relative stiffnesses κ.

It is clear from Fig. 7(a) that as the prestress level is increased, higher axial loads can be applied to the strut before the occurrence of first yield. In the case where $\tau = 1$, *i.e.* when the prestressing force is equal to the squash load $P_y = Af_y$ of the strut, the prestressed cable stabilizes the strut fully (*i.e.* prevents global buckling) for all slenderness values.

In Fig. 7(b), the effect of the relative stiffness κ is investigated for three different prestress levels. Generally, it is observed that, for a given prestress level, the first yield capacity of the member is not affected significantly by changes in κ; note that the influence of κ actually vanishes with increasing prestress level. This indicates that the first yield capacity of the prestressed member is not dependent on the characteristics of the cable [9]; instead, it is dependent solely on the level of prestress. Hence, as discussed in the following sub-section, the axial stiffness of the cable can be excluded from the formulation without affecting the obtained results significantly.

3.1.2. Excluding cable axial stiffness

An expression for determining the first yield capacity of the studied system in the case where $\kappa = 0$ is derived currently. This special case is relevant since, firstly, in practice it is difficult to provide fully rigid anchorage points for the cable and thus its effective axial stiffness is reduced by the flexibility of the anchorage. Secondly, if the system is applied in long-span structures, it is most likely that the length of the cable will be significantly larger than the length of the strut, and therefore the value of κ will be relatively small.

By setting $\kappa = 0$ in Eq. (28) and truncating the η^2 terms (since $\eta^2 \propto \epsilon^2$ and ϵ^2 is small currently), a simplified expression for the equilibrium path of the imperfect system in terms q can be obtained, thus:

$$\left[\lambda^2 - \eta(q-1)\right] = \left(1 - \frac{1}{q}\right) + \tau\lambda^2. \tag{31}$$

Solving Eq. (31) for q and substituting the result into Eq. (27) leads to the following expression for χ:

$$\chi = \frac{\tau+1}{2} + \frac{\eta+1}{2\bar{\lambda}^2} - \frac{1}{2\bar{\lambda}^2}\sqrt{[(\tau-1)\bar{\lambda}^2 - \eta + 1]^2 + 4\eta}, \tag{32}$$

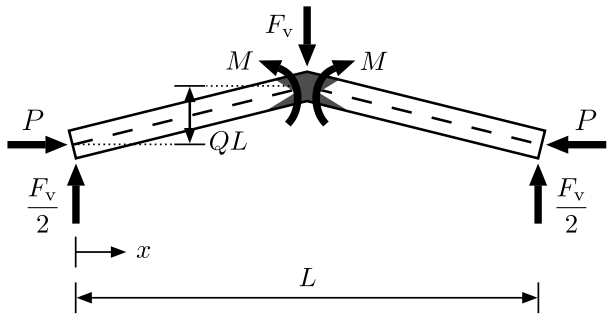
which, given the required non-dimensional parameters, can be readily evaluated to obtain the first yield capacity of the strut. It is worth noting that by setting $\tau = 0$ in Eq. (32) the classic Perry–Robertson expression is recovered. Furthermore, setting $\tau = 1 \implies \chi = 1$, *i.e.* the squash load of the strut is obtained, which agrees with the results shown in Fig. 7.

3.2. Rigid–plastic response

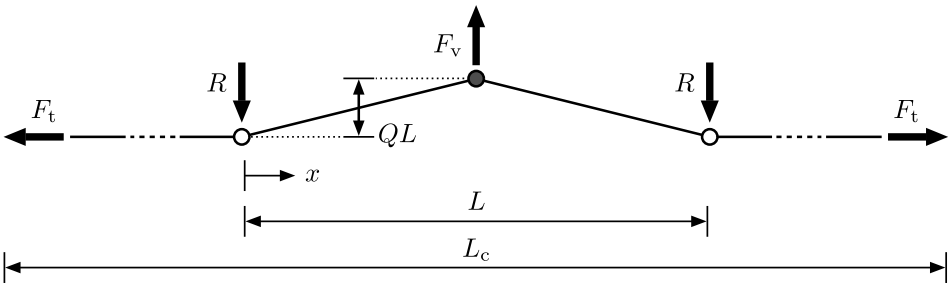
In the current section, it is assumed that, following the point of first yield, a plastic hinge develops at the midspan of the strut. In terms of equilibrium, the relationship between the applied external load and the lateral displacement at midspan is determined for two different plastic hinge models. First, an axial–flexural plastic hinge is assumed. Secondly, a flexural-only plastic hinge is considered. The latter is a good approximation of the former in cases where axial loads are small in comparison with the squash load of the strut. Moreover, it is shown to be useful in obtaining an estimate of the relative stiffness parameter κ at which the ultimate load switches from the load at first yield to a higher load corresponding to stable behaviour in the post-yield range, as determined from the rigid–plastic model.

3.2.1. Axial–flexural plastic hinge

To derive the relationship between the externally applied compression P and the lateral deflection of the strut at midspan QL, the free-body diagrams shown in Fig. 8 are used; R



(a) Rigid–plastic strut with plastic hinge at midspan



(b) Cable

Figure 8: Force diagrams of the rigid–plastic model with a plastic-hinge at midspan.

is the vertical reaction force at the strut supports due to stretching of the cable and F_v is the vertical equilibrium force at the location of the plastic hinge.

Using Fig. 8(a) and basic statics, the following relationship between the bending moment at midspan M and the applied forces is obtained:

$$M = \frac{F_v L}{4} - PLQ. \tag{33}$$

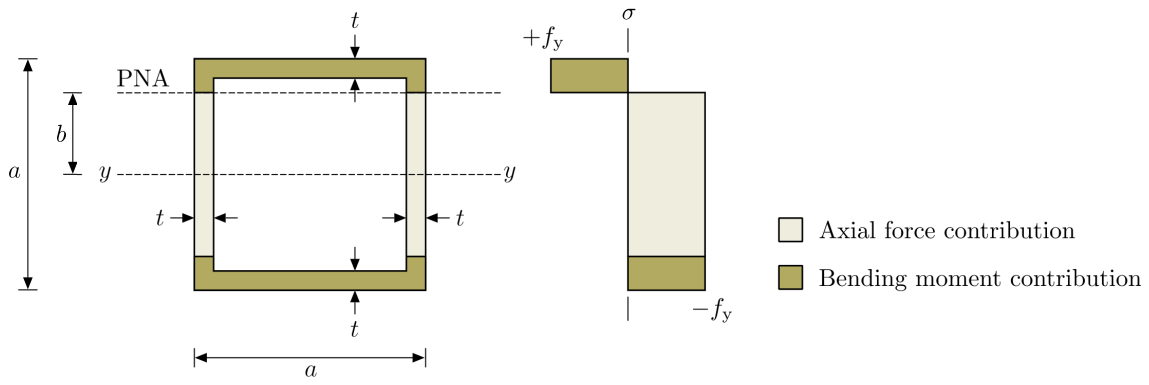
Furthermore, based on the equilibrium of forces in Fig. 8(b), where F_t is the total tensile force in the cable, and assuming small rotations, the initial prestressing force T can be related to F_v, such that:

$$F_v = 8k_c LQ^3 + 4TQ. \tag{34}$$

By substituting Eq. (34) into (33), an expression relating M to P and Q is obtained:

$$M = (2k_c LQ^2 + T - P)LQ. \tag{35}$$

To incorporate the axial–flexural plastic hinge into the model, it is necessary to derive an additional relationship between the axial force and the bending moment at the plastic hinge. For this purpose, a generalized fully plastic axial stress distribution is assumed at



(a) Square hollow section (b) Axial stress distribution

Figure 9: Fully plastic axial stress distribution; σ is the axial stress level with tensile stresses being positive.

the midspan of the strut, as shown in Fig. 9, where it is assumed that the central region of the cross-section resists the axial load while the two outer regions resist the second order moment due to the lateral deflection of the strut. The cross-section is assumed to be a square hollow section of side dimension a and wall thickness t; the plastic modulus can be seen to be equal to $W_{\rm pl} = a^3/4 - (a-2t)^3/4$.

Two cases must be distinguished. First, where the plastic neutral axis (PNA) resides within the web of the cross-section and, secondly, where it resides within the flange, *i.e.*:

$$M = -f_{\rm y}\left[W_{\rm pl} - \frac{t}{2}\left(\frac{P}{2f_{\rm y}t}\right)^2\right] \qquad \text{for} \quad b \leqslant a/2 - t, \tag{36}$$

$$M = -\frac{(P - f_{\rm y}A)(Af_{\rm y} - P - 2a^2 f_{\rm y})}{4af_{\rm y}} \qquad \text{for} \quad a/2 - t \leqslant b < a. \tag{37}$$

Finally, using Eq. (35) and the M versus P relationships given in Eqs. (36) and (37), the load–deflection relationship for the rigid–plastic model is obtained, such that:

for $b \leqslant a/2 - t$:

$$P = 4f_{\rm y}Lt\left[-Q + \sqrt{\frac{k_{\rm c}}{f_{\rm y}t}Q^3 + Q^2 + \frac{T}{2f_{\rm y}Lt}Q + \frac{W_{\rm pl}}{2L^2t}}\right], \tag{38}$$

and for $a/2 - t \leqslant b < a$:

$$P = 2f_{\rm y}aL\left[\left(\frac{A}{2aL} - \frac{a}{2L} - Q\right) + \sqrt{\frac{2k_{\rm c}}{f_{\rm y}a}Q^3 + Q^2 + \left(1 + \frac{T}{f_{\rm y}a^2} - \frac{A}{a^2}\right)\frac{a}{L}Q + \frac{a^2}{4L^2}}\right]. \tag{39}$$

For a given set of parameters, the relationships between the external compressive load and the tensile force in the cable with respect to the generalized lateral displacement of the strut are shown in Fig. 10. To ensure that all the tension stiffening effects originate

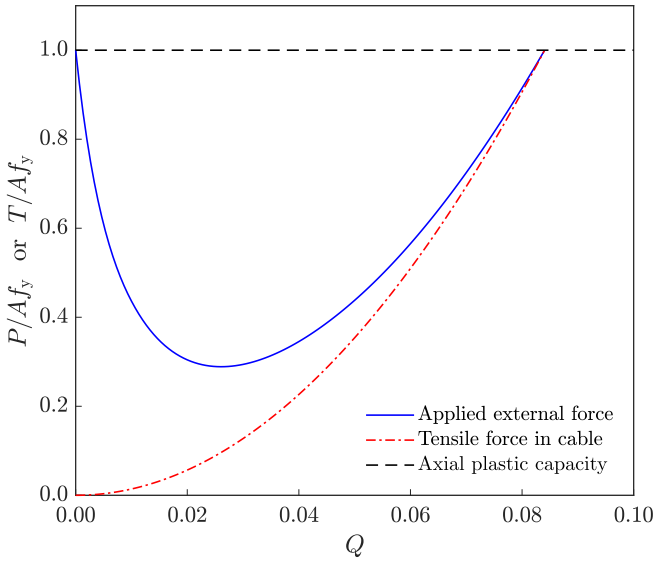


Figure 10: Sample result for the axial–flexural plastic hinge model. Variations of the external load P and tensile force in the cable T relative to the generalized lateral displacement of the strut Q.

only from the stretching of the cable, the initial prestressing force was chosen to be zero. From Fig. 10, two principal observations can be made; first, the squash load of the strut is not exceeded for any value of Q and, secondly, the curve for P has a negative slope for small values of Q, indicating that the rigid–plastic system is unstable at small lateral deflections. In contrast, at large deflections, the slope of the curve is positive, indicating that the system becomes stable. This coincides with the increase in the tensile force in the cable, as shown Fig. 10. It is therefore clear that the tensioning of the cable due to the lateral deflection of the strut is the stabilizing mechanism of the system.

Based on the axial–flexural plastic hinge model presented hitherto, two possible outcomes can occur after the point of first yield. The system will either transition into an unstable rigid–plastic mode and thus unload, as occurs in conventional struts [28] – in such a case the system is considered to have collapsed – or it will transition into a stable mode and collapse will occur by either failure of the cable in tension or by excessive plastic strains at the plastic hinge.

3.2.2. Flexural-only plastic hinge

Based on the analysis presented above, a simplified model that considers a flexural-only plastic hinge is derived herein. In this case, the contribution of the axial load to the cross-sectional stress distribution at the plastic hinge is ignored; hence, the bending moment within the plastic hinge is:

$$M = -f_{\mathrm{y}} W_{\mathrm{pl}}. \tag{40}$$

Substituting Eq. (40) into (35), the following relationship between the external compressive load and the lateral displacement at midspan is obtained:

$$P = 2k_c LQ^2 + \frac{f_y W_{pl}}{QL} + T. \tag{41}$$

Evidently, this relationship is simpler than those for the axial–flexural hinge model, as given in Eqs. (38)–(39).

Combining the results of the present section with those from Sections 2 and 3, the complete load–displacement curve can be obtained, as illustrated in Fig. 11. A linear

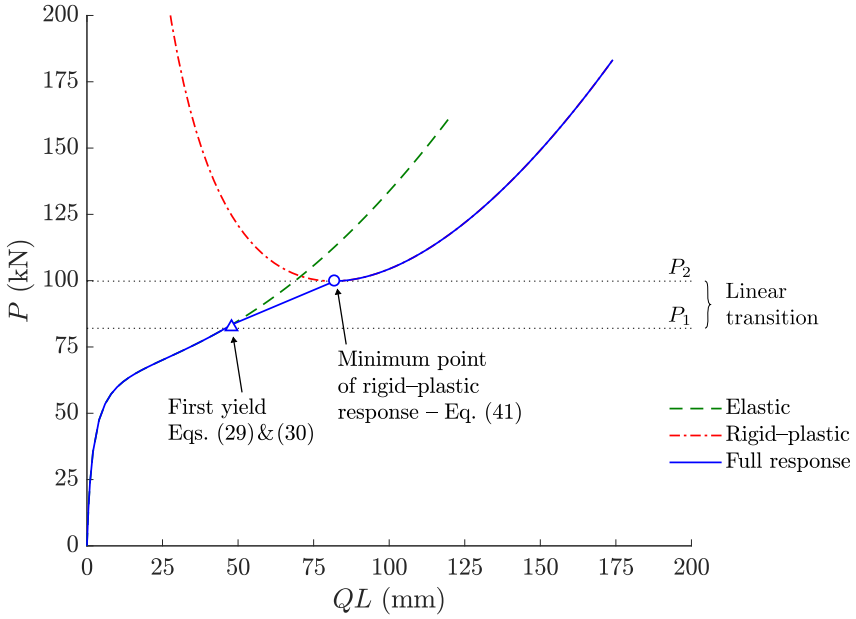


Figure 11: Equilibrium path of the sample system based on the developed elastic, first yield and rigid–plastic (flexural-only) responses.

transition is assumed between the point of first yield P_1 and the minimum point of the rigid–plastic response P_2 of the system. In the present paper, this transition is defined through linear interpolation between the P_1 and P_2 loads, when $P_2 > P_1$. In this example, owing to the high relative stiffness parameter ($\kappa = 3153$), the response following the occurrence of first yield remains stable.

3.3. Limiting value of relative stiffness

As identified in Section 3.2, following the occurrence of first yield the system may unload and thus collapse. This type of failure occurs when the system transitions from the point of first yield into an unstable rigid–plastic response and it is marked by a low axial stiffness of the cable (*i.e.* a low value of κ). Currently, a criterion for identifying the limiting value of the relative stiffness $\kappa = \kappa_{\text{lim}}$, at which the system transitions from an unstable to a stable rigid–plastic response, is proposed.

The proposed criterion is based on the assumption that, if the applied load corresponding to the minimum point of the rigid–plastic load–displacement curve P_2 is lower than the applied load at the point of first yield P_1, then the system will unload after the point of first yield. Based on this assumption, κ_{lim} corresponds to the value of κ that results in the same applied load at the two aforementioned points. An illustration of the proposed criterion is shown in Fig. 11, where the triangle indicates the point of first yield and the circle indicates the minimum point of the rigid–plastic curve. The latter can be found by differentiating Eq. (41) with respect to Q, setting the resulting expression equal to zero, and subsequently substituting the result back into the original equation to obtain the expression for P_2, *i.e.*:

$$P_2 = \frac{3}{2}\left[\frac{4k_{\text{c}}}{L}(f_{\text{y}}W_{\text{pl}})^2\right]^{1/3} + T. \tag{42}$$

As defined in Eq. (30), P_1 is a function of the buckling reduction factor χ, which is itself a function of κ. Hence, by equating the expression for P_1 with Eq. (42), the limiting condition of $\kappa = \kappa_{\text{lim}}$ can be formulated as $P_2 = \chi(\kappa_{\text{lim}})Af_{\text{y}}$, where $\chi(\kappa)$ can be obtained numerically using the procedure described in Section 3.1.1.

With the proposed criterion, the relative stiffness parameter can indicate whether the studied system would remain stable after the point of first yield or whether the first yield capacity is a good prediction of the collapse load.

4. Numerical modelling

In the present section, numerical results obtained from finite element (FE) models developed in ABAQUS [29] are presented. The FE results are used to validate the analytical models developed in the previous sections and to demonstrate the application of the studied structural concept in the case of a prestressed hangar roof truss. The special case where $\kappa = \kappa_{\text{lim}}$ is also explored.

4.1. Verification of analytical model for occurrence of first yield

In the developed FE model, a $50 \times 50 \times 5$ mm square hollow section was employed for the strut, while the radius of the cable was chosen to be 6 mm. The constitutive response of the strut was assumed to be elastic, perfectly–plastic with yield stress 355 N/mm^2 and Young's modulus 210 kN/mm^2. A linearly elastic material response was adopted for the cable; hence, the stress level within the cable was monitored to ensure it did not exceed 1860 N/mm^2, which is the typical tensile strength for high-strength steel cables [9, 24]. The lengths of both the strut and the cable were taken as $L = L_{\text{c}} = 3000$ mm with a global imperfection of normalized amplitude $\epsilon = 1/1500$ being imposed along their length. The cubic B23 [29] beam elements and the linear T2D2 [29] truss elements were employed to model the strut and the cable respectively.

The unbonded connection between the two structural components (*i.e.* the tube and the cable) was modelled using constraint equations [29] orientated only in the direction normal to the centreline of the strut; in this manner, the cable was allowed to elongate freely

along its entire length [8, 9]. The boundary conditions at the two ends of the components are shown in Fig. 3. To demonstrate the effect of the tensioning of the cable due to the increase in the lateral deformations of the strut, the initial prestressing force was set to zero. Moreover, with the aim of achieving the relative stiffness parameter of $\kappa = 1000$, the Young's modulus of the cable was set to be equal to $E_c = 63.5$ kN/mm^2, the lower stiffness reflecting the response of a spiral strand, rather than a solid, cable.

The FE result obtained using the modified Riks arc-length solver [30], which is widely used in the analysis of geometrically and materially nonlinear structural problems (*e.g.* [31, 32]), is shown in Fig. 12 in terms of the load–displacement response of the system. The

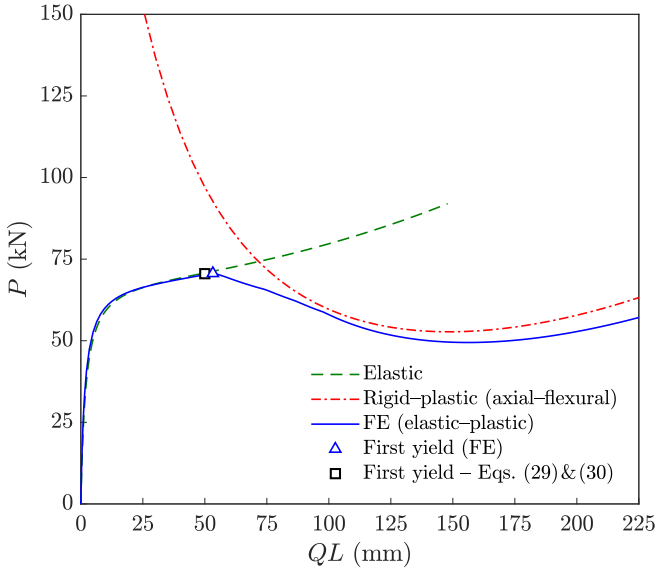


Figure 12: Comparison between the analytical results, obtained using the developed elastic and rigid–plastic (axial–flexural) models, and the results of the FE model, for the case of $\kappa = 1000$.

analytical results corresponding to the elastic and rigid–plastic (axial–flexural) responses of the system are also shown; these were obtained using Eqs. (13) and Eqs. (38)–(39) respectively. Overall, the asymptotic nature of the FE response relative to the two analytical predictions demonstrates the excellent agreement between the models.

With regards to the point of first yield, the relative error between the FE result and the analytical prediction is 0.7%, while, with respect to the minimum point of the rigid–plastic response, the relative error is 2.9%. After the point of first yield, the structure becomes unstable, but after a significant lateral displacement, the system restabilizes. The failure mode in this example is essentially a snap-though instability; thus, under dead loading, the structure would dynamically jump at constant load from the point of first yield to the rising equilibrium branch to the right.

4.2. Verification of analytical model for stable post-yield cases and κ_{lim}

In the example presented below, the relative stiffness parameter κ was chosen to be equal to its limiting value κ_{lim}, as defined in Section 3.3. Consequently, the results would

be expected to show a neutrally stable equilibrium path after the point of first yield. To obtain the desired value of $\kappa_{\text{lim}} = 1750$, the Young's modulus of the cable was set to a value of $E_{\text{c}} = 110$ kN/mm^2. In Fig. 13, comparisons between the two developed plastic hinge

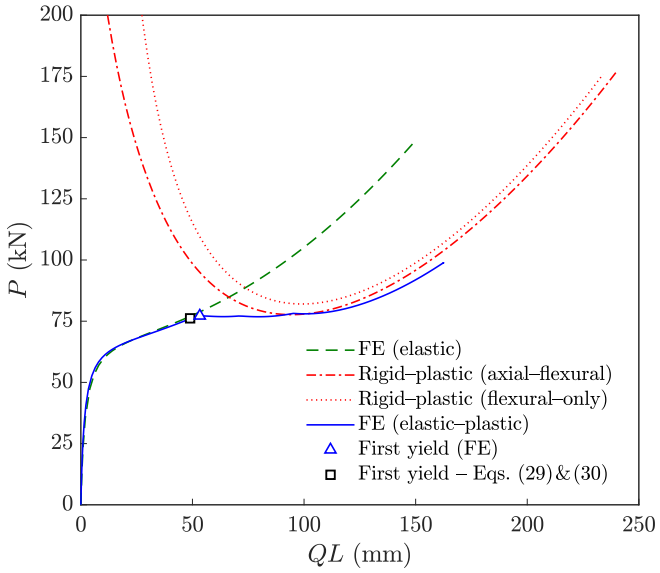


Figure 13: Comparison between the analytical results, obtained using the developed elastic and rigid–plastic (axial–flexural and flexural-only) models, and the results of the FE model, for the case of $\kappa = \kappa_{\text{lim}} = 1750$.

models, namely axial–flexural and flexural-only, and the FE model are shown in terms of the load–displacement response of the modelled system. The FE results were obtained using both elastic and elastic–plastic material definitions.

Comparing the analytical results with those from the FE model, it is observed that, overall, very good agreement is achieved. In the current example, since the axial load applied to the strut is low relative to the squash load, the flexural-only model is also seen to give accurate predictions. Furthermore, the estimated value of κ_{lim} agrees very well with the predicted neutrally stable response following the point of first yield; this verifies the method for determining the value of κ_{lim}, as proposed in Section 3.3.

4.3. Analysis of prestressed hangar roof truss

Application of the studied structural concept is demonstrated herein by modelling the behaviour of a prestressed long-span aircraft hangar, such as the one shown in Fig. 2, when subjected to gravity loading. The hangar comprises steel roof trusses, spaced at 5 metre intervals and with a flat top chord profile. The prestressed cables are housed within the top chord of the trusses and deviated by struts towards external anchorage blocks in the ground. The stabilizing action offered by the presence of the prestressed cables is thus explored.

4.3.1. Characteristics of FE model

A representation of the developed FE model is shown in Fig. 14. Assuming full bracing between the individual trusses, out-of-plane deformations were not considered herein and thus a planar model was created. Furthermore, owing to the symmetry of the truss, only half of the structure was modelled. The FE techniques employed to model the structural components, connections and boundary conditions are the same as those presented in Section 4.1. Note that initial imperfections of magnitude $L/1000$ were introduced along the members of the top chord, while all the joints between the steel members of the truss were modelled as rigid.

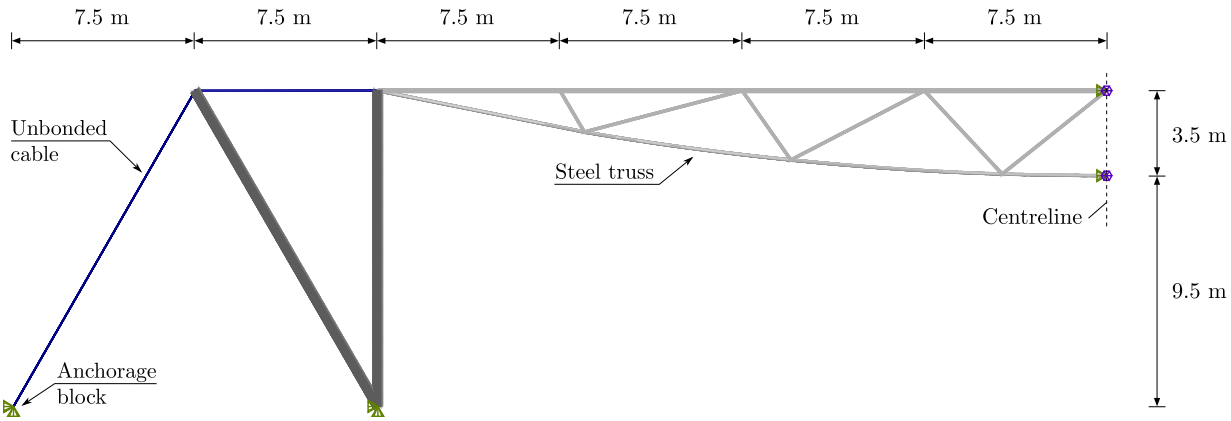


Figure 14: FE model of the studied prestressed hangar roof truss with symmetry imposed.

As shown in Fig. 14, the top chord of the truss comprises eight 7.5 m long elements, to give a total span of 60 m, while the maximum depth of the truss at midspan is 3.5 m. The top chord has a $160 \times 160 \times 10$ mm square hollow section, material yield strength $f_y = 355$ N/mm^2 and Young's modulus $E = 210$ kN/mm^2. The cross-sections of the diagonal and bottom chord elements were selected such that they would not fail before the top chord. The cable has a cross-sectional area $A_c = 1650$ mm^2, a total length $L_c = 105$ m and Young's modulus $E_c = 160$ kN/mm^2. Finally, an initial prestressing force $T = 1400$ kN, which is equal to approximately two thirds times the squash load of the strut, was applied by means of thermal loading [8, 9].

The gravity loading on the structure was assumed to be uniformly distributed with magnitude 2.6 kN/m^2; this is equivalent to 13 kN/m along an individual truss. The distributed load was imposed using concentrated loads at the junctions between the top chord and the diagonals. For the sake of simplicity no other loads were applied to the structure.

4.3.2. Analytical predictions

To analyse the behaviour of the truss structure, the top chord element adjacent to the midspan is considered herein. Using statics, it can be approximated that, under the design loading of $p_{Ed} = 2.60$ kN/m^2, this critical element is subjected to an axially compressive force $P_{Ed} = 1671$ kN.

To predict the failure mode of the critical member, the relative stiffness concept is subsequently utilized. Assuming that the buckling length of the member is equal to 7.5 m, and given that the total length of the cable is 105 m, the relative stiffness parameter is obtained using Eq. (23) as $\kappa = 223.5$. Meanwhile, by utilizing the method described in Section 3.3, the limiting value $\kappa_{\text{lim}} = 594$ can be determined. Since $\kappa < \kappa_{\text{lim}}$, failure at the point of first yield is predicted.

As discussed in Section 3.1.2, since the value of κ is relatively small, the axial stiffness of the cable can be ignored in the calculation of the axial capacity of the member. Hence, using Eqs. (32) and (30), the buckling reduction factor and first yield capacity of the critical member can be predicted as $\chi = 0.87$ and $P_1 = 1847$ kN respectively; this corresponds to a distributed loading of magnitude $p_1 = 2.87$ kN/m^2. Therefore, the top chord is expected to resist the design load $P_{\text{Ed}} = 1671$ kN. In this example, the normalized imperfection magnitude η was determined using the Eurocode 3 designation [27], *i.e.* $\eta = \alpha(\bar{\lambda} - 0.2) \not< 0$, where $\alpha = 0.21$ for hot-rolled tubular members.

4.3.3. Analysis of FE results

The response of the FE model, as obtained by performing a Riks analysis [30] on the truss structure, is shown in Fig. 15, where three different cases are presented: (i) no cable;

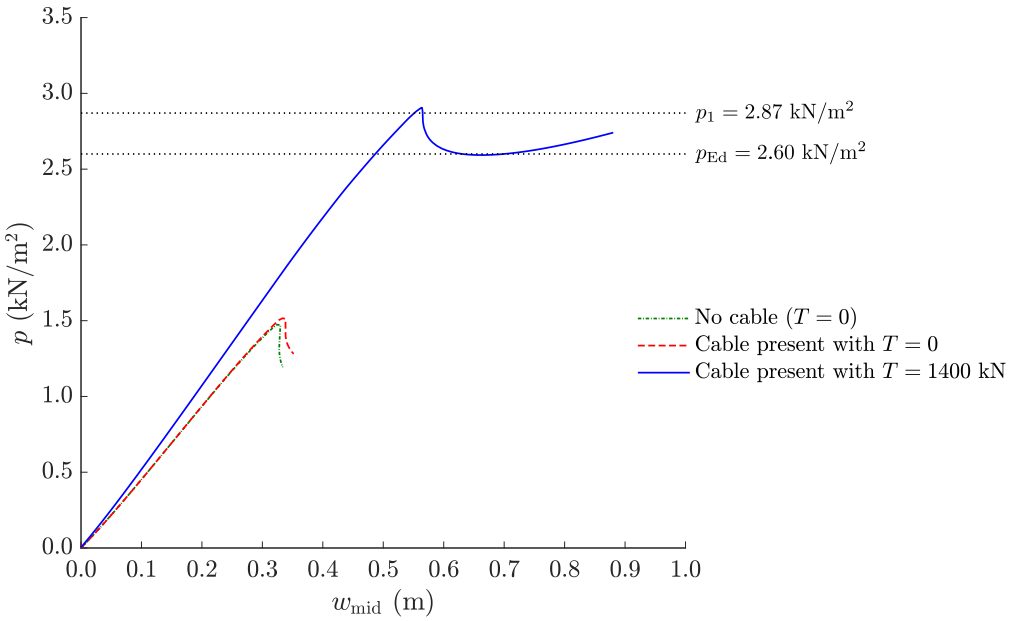


Figure 15: FE results from the prestressed hangar model; applied loading p versus vertical displacement at midspan w_{mid}.

(ii) cable present without prestress; (iii) cable present with prestress.

Firstly, it can be observed that the difference between the responses of cases (i) and (ii) is minimal. This is because, as discussed in Section 3.1.1, the first yield capacity is not affected significantly by the addition of the cable when prestressing is not applied. In contrast, in case (iii), with the application of prestress, the occurrence of first yielding in

the critical member was delayed, thus increasing the capacity of the structure significantly. Specifically, in this case, a nearly two-fold increase (97%) in the ultimate capacity of the structure was attained from the addition of the prestressed cable.

Secondly, it can be observed that, when no prestressing was applied, the structure failed at a much lower load level than the specified design load of $p_{\text{Ed}} = 2.60$ kN/m^2. Meanwhile, the application of the prestressing force enabled the structure to withstand loads above the design load. Overall, comparing the ultimate point of the prestressed model $p_{\text{FE}} = 2.90$ kN/m^2 with the analytical prediction $p_1 = 2.87$ kN/m^2, it can be seen that excellent agreement was achieved between the FE and analytical results.

Finally, as predicted in Section 4.3.2, the failure mode in all three cases corresponds to an instability in the top chord at the point of first yield. The mode of failure in the case of the prestressed hangar is illustrated in Fig. 16. Clearly, failure was triggered by buckling of the top chord segment adjacent to the hangar midspan.

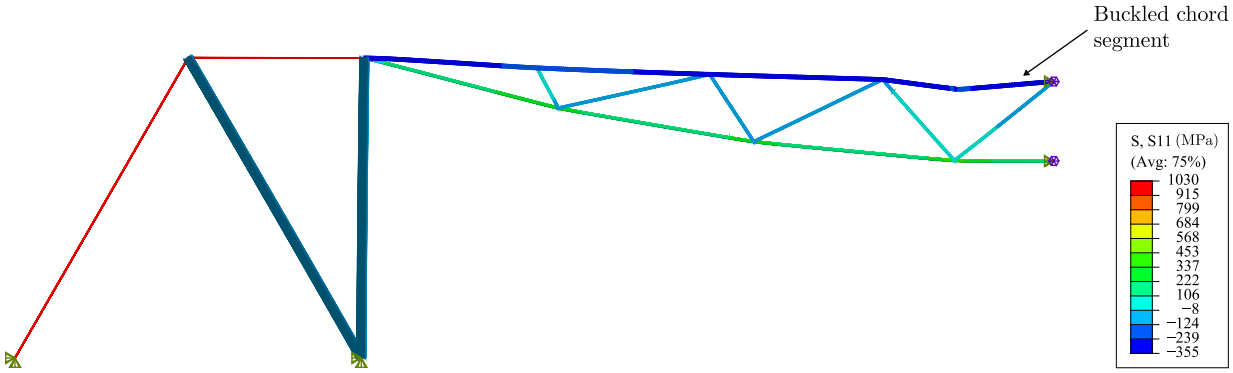


Figure 16: Failure mode in the FE model, demonstrating buckling of a top chord segment.

5. Conclusions

The utilisation of prestressed cables can enhance the efficiency of long span steel structures by prestressing the structural elements against the subsequently applied external loading and by carrying loads through catenary action. Previous research has focused on cases where the prestressed cables are anchored against the structure itself, with the system therefore being mutually equilibrating. In contrast, the notion of employing externally anchored prestressed cables to enhance the stability of steel truss compression elements has been explored herein. The studied structural system comprises a tubular strut subjected to an external compressive force and housing a prestressed cable that is allowed to elongate freely and is anchored independently of the strut.

By utilizing energy methods, analytical expressions describing the elastic response of the system have been developed first. These expressions define the pre-buckling and post-buckling equilibrium paths of both the perfect and the imperfect systems. Subsequently, a numerical example has demonstrated that the higher the prestressing force, the higher the

elastic critical buckling load of the system and that its post-buckling stability is independent of the initial prestress level. Meanwhile, it has been shown that increasing the length of the strut decreases the elastic critical buckling load of the system but, in turn, increases its post-buckling stiffness.

The first yield and rigid–plastic responses of the system have also been studied. The former was examined through extension of the well-known Perry–Robertson concept. An expression for the first yield capacity of the system was therefore derived. Furthermore, it has been demonstrated that the first yield capacity of the member is not affected significantly by the characteristics of the cable and that the increase in capacity is driven by the prestress level. Subsequently, the formation of an axial–flexural or a flexural-only plastic hinge at the strut midspan was studied by means of a rigid–plastic analysis. It has been shown that whether the system remains stable after the point of first yield or whether it collapses depends on the relative stiffness parameter (defined currently as the ratio between the axial stiffness of the cable and the bending stiffness of the strut); an expression for predicting its limiting value was therefore developed.

A finite element (FE) model has been employed to illustrate application of the studied structural concept to the case of a prestressed roof truss designed for a hypothetical aircraft hangar. The cable was housed within the top chord of the truss and was assumed to be attached to external anchorage blocks in the ground. A nearly two-fold increase in the ultimate capacity of the truss structure owing to the addition of the prestressed cable was demonstrated. The FE results have also been compared with the corresponding analytical predictions with excellent agreement being achieved. There is clearly more scope to optimize the effects discussed currently in future work. Furthermore, the concept of employing externally anchored prestressed cables to restrict lateral-torsional buckling effects in the case of long-span steel flexural members will be explored in future studies.

References

[1] PT Architectural Technology Pty Ltd, http://www.pt-technology.com.au/home/track-record.aspx (accessed 22 September 2019).

[2] J. Gosaye, L. Gardner, M. A. Wadee, M. E. Ellen, Compressive behaviour and design of prestressed steel columns, Structures 5 (2016) 76–87.

[3] G. Magnel, Prestressed steel structures, The Structural Engineer 28 (11) (1950) 285–295.

[4] P. G. Hoadley, Development and use of prestressed steel flexural members: Part 2 - Prestressing by means of high strength steel wires or bars, Subcommittee 3 on Prestressed Steel of Joint ASCE-AASHO Committee, Journal of the Structural Division, ASCE 94 (9) (1968) 2035–2042.

[5] M. S. Troitsky, Z. A. Zielinski, N. F. Rabbani, Prestressed-steel continuous-span girders, Journal of Structural Engineering, ASCE 115 (6) (1989) 1357–1370.

[6] B. Belletti, A. Gasperi, Behaviour of prestressed steel beams, Journal of Structural Engineering, ASCE 136 (9) (2010) 1131–1139.

[7] M. E. M. Kambal, Y. Jia, Theoretical and experimental study on flexural behavior of prestressed steel plate girders, Journal of Constructional Steel Research 142 (2018) 5–16.

[8] N. Hadjipantelis, L. Gardner, M. A. Wadee, Prestressed cold-formed steel beams: Concept and mechanical behaviour, Engineering Structures 172 (2018) 1057–72.

[9] N. Hadjipantelis, L. Gardner, M. A. Wadee, Finite element modeling of prestressed cold-formed steel beams, Journal of Structural Engineering, ASCE. 145 (10) (2019) 04019100.

[10] N. Hadjipantelis, L. Gardner, M. A. Wadee, Design of prestressed cold-formed steel beams, Thin-Walled Structures 140 (2019) 565–578.

[11] D. Saito, M. A. Wadee, Post-buckling behaviour of prestressed steel stayed columns, Engineering Structures 30 (2008) 1224–1239.

[12] A. I. Osofero, M. A. Wadee, L. Gardner, Experimental study of critical and post-buckling behaviour of prestressed stayed columns, Journal of Constructional Steel Research 79 (2012) 226–241.

[13] R. R. de Araujo, S. A. L. de Andrade, P. C. G. d. S. Vellasco, J. G. S. da Silva, L. R. O. de Lima, Experimental and numerical assessment of stayed steel columns, Journal of Constructional Steel Research 64 (9) (2008) 1020–1029.

[14] M. Serra, A. Shahbazian, L. S. da Silva, L. Marques, C. Rebelo, P. C. G. d. S. Vellasco, A full scale experimental study of prestressed stayed columns, Engineering Structures 100 (Oct) (2015) 490–510.

[15] J. Yu, M. A. Wadee, Mode interaction in triple-bay prestressed stayed columns, International Journal of Non-Linear Mechanics 88 (2017) 47–66.

[16] M. S. Troitsky, Prestressed steel bridges: theory and design, Van Nostrand Reinhold, New York, 1990.

[17] H. Li, L. C. Schmidt, Posttensioned and shaped hypar space trusses, Journal of Structural Engineering, ASCE 123 (2) (1997) 130–137.

[18] B. M. Ayyub, A. Ibrahim, Post-tensioned trusses: Reliability and redundancy, Journal of Structural Engineering, ASCE 116 (6) (1990) 1507–1521.

[19] M. E. Ellen, J. Gosaye, L. Gardner, M. A. Wadee, Design and construction of long-span post-tensioned tubular steel structures, in: Tubular Structures XIV - Proceedings of the 14th International Symposium on Tubular Structures, 2012, pp. 687–693.

[20] M. J. Clarke, G. J. Hancock, Finite-element nonlinear analysis of stressed-arch frames, Journal of Structural Engineering, ASCE 117 (10) (1991) 2819–2837.

[21] M. J. Clarke, G. J. Hancock, Tests and nonlinear analyses of small-scale stressed-arch frames, Journal of Structural Engineering, ASCE 121 (2) (1995) 187–200.

[22] S. Afshan, M. Theofanous, J. Wang, M. Gkantou, L. Gardner, Testing, numerical simulation and design of prestressed high strength steel arched trusses, Engineering Structures 183 (2019) 510–522.

[23] J. Wang, S. Afshan, L. Gardner, Axial behaviour of prestressed high strength steel tubular members, Journal of Constructional Steel Research 133 (2017) 547–563.

[24] J. Gosaye, L. Gardner, M. A. Wadee, M. E. Ellen, Tensile performance of prestressed steel columns, Engineering Structures 79 (2014) 234–243.

[25] J. M. T. Thompson, G. W. Hunt, A general theory of elastic stability, Wiley, Chichester, 1973.

[26] H. G. Allen, P. S. Bulson, Background to buckling, McGraw-Hill, 1980.

[27] EN 1993-1-1, Eurocode 3: Design of steel structures - Part 1-1: General rules and rules for buildings, Brussels: European Committee for Standardization (CEN), 2006.

[28] J. Wang, L. Gardner, Flexural buckling of hot-finished high-strength steel SHS and RHS columns, Journal of Structural Engineering, ASCE 143 (6) (2017) 04017028.

[29] ABAQUS, Abaqus analysis user's guide - online documentation, Version 6.14-2, Dassault Systemes Simulia Corp.

[30] E. Riks, An incremental approach to the solution of snapping and buckling problems, International Journal of Solids and Structures 15 (7) (1979) 529–551.

[31] M. Kucukler, L. Gardner, L. Macorini, Lateral-torsional buckling assessment of steel beams through a stiffness reduction method, Journal of Constructional Steel Research 109 (2015) 87–100.

[32] P. Kyvelou, C. Kyprianou, L. Gardner, D. A. Nethercot, Challenges and solutions associated with the simulation and design of cold-formed steel structural systems, Thin-Walled Structures 141 (2019) 526–539.